DESERT 2021, 26(2): 251-265
DOI: 10.22059/jdesert.2021.318414.1006806

RESEARCH PAPER

Combination of Spectral Indices of OLI and TIRS Sensor and Magnetic Induction Data to Estimate Spatial Variation of Soil Salinity

Hamid Reza Matinfar*, Nava Kianian, Sassan Ahmadi

Soil Science Dept., Lorestan University, Khorramabad, Iran

Received: 02 February 2021, Revised: 13 April 2021, Accepted: 07 June 2021

Abstract
Soil salinity and alkalinity are believed to be among the most important soil degradation processes, specifically in arid and semi-arid regions. Identification and monitoring of salinity is also necessary for land and environmental management. Continuous salinity monitoring is traditionally costly and time-consuming while using satellite data and combining them with magnetic induction data could be an alternative to the traditional method. The present study aimed to evaluate spectral indicators and identify saline soils and spatial changes via the data of the [2]EM38. The study area was conducted in Ghahavand plain located in Hamedan Province. In this study, Landsat 8 satellite data were used. The image was georeferenced with the image-to-map method with more than 12 control points and accuracy of fewer than 0.4 pixels. Atmospheric correction was performed through the black body method. Soil sampling of 37 points was performed and 86 points were read using an electromagnetic induction device. The soil samples were transferred to the laboratory and passed through a 2-mm sieve. The sample analysis was performed according to standard methods. Using protomorphic units based on visual interpretation of OLI 543 false-color composite image and field observations, a total of nine homogeneous units were identified in the region using these units as training regions for supervised classification. The results revealed that the detection of soil salinity in the visible spectrum (blue, green, and red bands) is feasible. Bands 5, 6, and 7 could be useful for differentiating salty white crust lands from salty gray crust lands. In the reflective bands, the white and smooth crust lands exhibited the highest reflectance. The results of classification accuracy showed that the highest total accuracy was 90.0 and the kappa coefficient was 80.45 when bands 2, 3, 4, 5, 6, 7, 10, and 11 were used and shallow and abandoned plowed lands had the lowest accuracy. Furthermore, the final model of salinity estimation implied that SI6 and SI11 indicators and electromagnetic induction vertical measurements (EMv) were the most suitable variables for estimating salinity spatial changes.

Keywords: Soil salinity, Landsat 8, Spectral indices, Magnetic induction

Introduction

Soil salinity and alkalinity are among the most important soil destructive processes, especially in arid and semi-arid regions (El Harti, 2016; Ibrahim, 2016; Kumar, 2018). The regions affected by salinity are highly susceptible to temporal and spatial changes in climate and hydrology. Soil salinity, like other natural hazards, such as earthquakes and landslides, cannot be damaged quickly, but is considered a serious environmental hazard (Yu et al., 2010). About 2 mega hectares of

* Corresponding author e-mail: matinfar.h@lu.ac.ir
[2] electromagnetic induction device

agricultural lands become salty every year in the world (Abbas et al., 2013). According to the estimations, 7% of the world's lands are salty and 3% are very salty or alkaline (Alavi-Panah, 2006). In Iran, about 15% of the country's lands are salty soils with varying degrees of salinity. The speed of salinization of land is high in some countries, such as Iran, Egypt, and Argentina. Therefore, the identification and monitoring of salty regions are necessary for controlling land degradation behavior and its sustainable management, particularly in semi-arid regions with poor climate conditions and increased population.

Traditional methods for collecting data and studying soil are time-consuming and costly. Today, with the advancement of science, the use of new technologies, such as receiving and processing satellite data, through the use of software and information processing systems, such as geostatistic, plays an important role in the management of water and soil resources. Salty and alkaline soils in the visible and infrared regions of the spectrum of electromagnetic waves have a certain spectral reflectance that can be used to determine soil salinity. In addition, a high correlation was found between soil reflectance and soil characteristics, including mineralogy, organic matter, moisture content, and salinity (Rao et al., 1995). In a similar study conducted by Mougenot et al. (1993), the results indicated that salinity is one of the factors affecting the reflectance of soil in remote sensing studies. Farifteh et al. (2006) also conducted studies on the correlation between spectral indicators calculated by satellite images and field data in the country. The remote sensing methods have been used in several studies for estimating soil salinity in arid and semi-arid regions (AzabDaftari et al., 2016; Matinfar et al., 2011; Nawar et al., 2014). Hafyani et al. (2019) modeled regional soil salinity in Morocco with Landsat 8 satellite imagery and compared it with field data through linear regression. They showed that remote sensing was good for soil salinity modeling and providing soil salinity mapping with good correlation coefficients ranged from 0.53 to 0.75. The basis of the application of salinity indicators is the variability of spectral properties based on the variability of soil characteristics, vegetation, and other environmental factors. Allbed et al. (2014) isolated three sites according to the visual interpretation of the false-color images and field data in an area affected by salinity. In their study, vegetation index and 12 salinity indicators were examined for salinity evaluation. They found that salty and dry soils and soft soils with a thin salt crust had a higher spectral reflectance than wet cracked salty soils with dark crust in the visible and near-infrared spectral spectrum. They also reported that SAVI[3], NDSI[4], and SI-T indicators derived from IKONOS images were conducive to evaluating and analyzing salty lands with vegetation.

In general, it has been found that NDSI and SI-T indicators were highly useful for evaluating salty lands in arid regions with low vegetation. In the same study, it was reported that vegetation indicators, such as SAVI, can be useful in regions with bulk vegetation. AbdelRahman et al. (2019), using drilled 90 soil profiles and 30 underground water samples, prepared maps of surface soil salinity changes as well as land use in 2002 and 2017. They showed that the use of spectral indicators could be effective in evaluating the status of groundwater using salinity. Abuelgasim and Ammad (2019) utilized Landsat 8 OLI sensor images and adjusted salinity indicators in near-infrared wavelengths and short wavelengths in a dry and semi-arid climate. It was concluded that the newly adjusted indicators had an overall accuracy of 60%. This is true if the old indicators' accuracy was 50%. Therefore, the model derived from the new indicators with six salinity classes was more efficient in estimating salinity levels. The application of band combinations for calculating indicators will increase the accuracy of salinity estimation in remote sensing studies. In

[٣] Soil Adjusted Vegetation Index

[٤] Normalized Difference Vegetation Index

this regard, Allbed et al. (2013), in a study on soil salinity modeling in a region of Saudi Arabia, showed that the combination of IKONOS red band and salinity indicators is highly conducive to providing a soil salinity map.

The use of thermal data could have a significant effect on the study of ground phenomena, including determining soil salinity reflectance. Additionally, El Harti (2016) showed a high correlation between soil salinity and SI using a combination of TM[5] and OLI[6] sensors of Landsat satellite and thermal bands. In other previous studies, green and red and near-infrared TM bands have indicated a high correlation with soil salinity map in Saudi Arabia (Asfaw et al. 2016). Rahmati and Hamzehpour (2017) examined soil salinity with information from satellite images and ground samples. They sampled 188 points in an area of 5000 hectares in the west of Lake Uremia. The results of the multivariate regression showed a high correlation coefficient (0.875) between salinity indicators and ground data. Another method for measuring soil salinity via new techniques is the electromagnetic induction device. Being easily carried, no need for sampling, and being time-effective are among the advantages of the device. In a study conducted in Australia, researchers could measure the EC (electrical conductivity) of 40 points per day using this device (Williams et al., 1982). Various models of this device are marketed.

Numerous studies have been conducted on the use of electromagnetic induction device EM38 to evaluate and determine soil salinity (Barbiero et al., 2001; Song et al., 2002). The results are developed as equations that relate readings of the device to the electrical conductivity of water-soil ratios, saturation paste, and EC of soil mass at different depths. Johnston (1996) used the EM38 device in Africa to monitor salinity. In this study, EM38 was found to be a good tool for providing salinity map. However, it requires the simultaneous use of GPS (global positioning system). In India, similar efforts have also been made and it has been argued that by calibrating and applying the proper equations, EM38 can be an efficient tool for rapid identification surveys across the country (Sharma and Gupta, 2000). According to their results, it seems as though the use of this device is cost-effective by emphasizing the mapping of salt-bearing soils in India. The present study aimed to evaluate spectral indicators for the identification of saline soils and determine the relationship between these indicators and electromagnetic induction data. In addition, Provide an integrated model of indicators and magnetic induction data to prepare soil salinity map.

Materials and Methods

Study area

The study area is located in Hamedan Province. The Ghare Chai River Basin is 5845 square kilometers and the major part is located outside Hamedan Province and in Markazi and Qom Provinces. Ghahavand plain is located on the northern slope of Alvand Mountain and East longitude of 9' 49 °-48° 58' and north latitude of 57' 34°-25' 34°; from the north, it is limited to Razan-Famenin plain, from the east to Daqdaq, Enjili, and Sefid mountains, from the west to Ghezeldaq and Qardash mountains, and from the south to the vast Shara Plain in Markazi Province (Figure 1). This area is physiographically one of flood plains and lowlands with the mean elevation of 1650 m above the sea level, the mean annual rainfall of 260 mm, the mean annual temperature of 11.79 °C, and the mean annual evaporation rate of the surface of the pan evaporation of 2020 mm. The region's climate is semi-arid according to De Matron Method and cold arid according to Amberge

[5] Thematic Mapper

[6] Operational Land Imager

method. According to the field studies, about 50% of the lands are under cultivation and the rest of the lands had no agricultural and horticultural uses. The dominant cultivation is rain-fed wheat and barley and alfalfa.

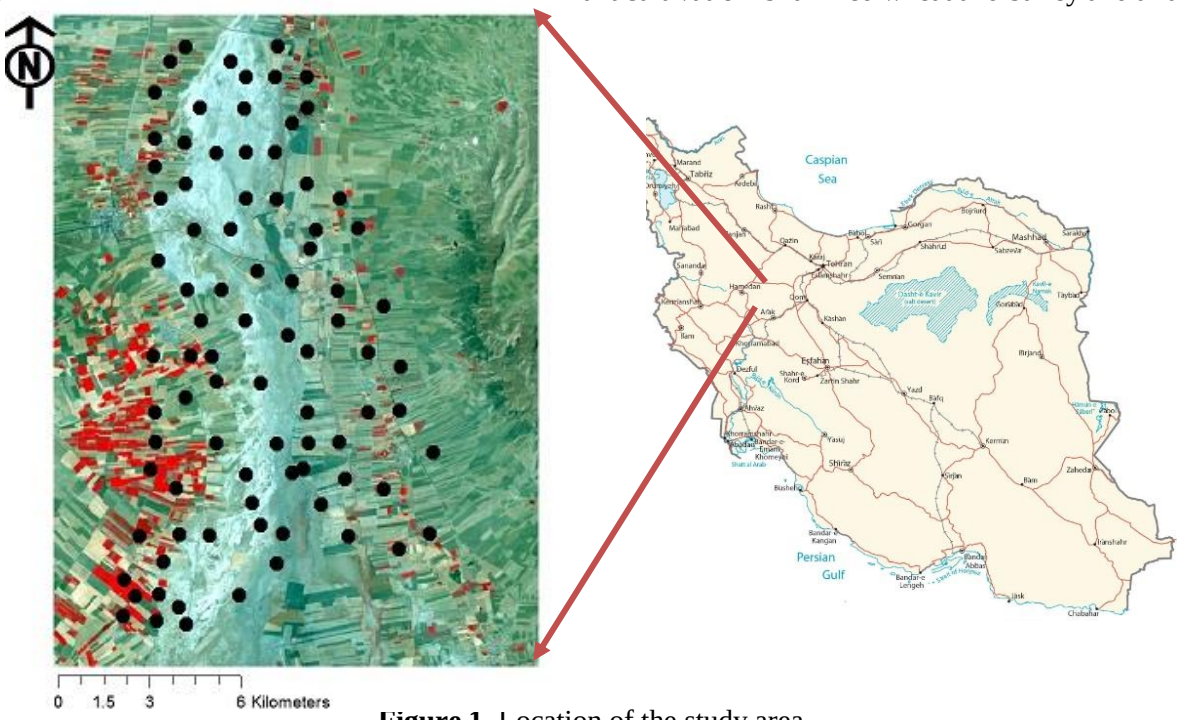

Figure 1. Location of the study area

Data

In this study, satellite images, ground data, and electromagnetic induction device data were used. EM38 is specifically designed for salinity examination in terms of agriculture and could be utilized at high speeds. This device is very light (2.5 kilograms in weight) and small (1 meter in length) and has acceptable durability. EM38 employs the principles of electromagnetic induction and can measure the electrical conductivity of the soil mass in milliseconds per meter on the horizontal and vertical surfaces. (Figure 2).

To select the satellite image, we attempted to select the hottest month of the year in order to have the maximum evaporation and as a result, the maximum accumulation of salts on the surface of the soil. In the present study,in order to evaluate the satellite data capability of the identification and separation of salty soils, nine Landsat 8 bands digital data were used collected in August 2013. In several studies, researchers have used Landsat 8 satellite images for estimating soil salinity (Forkuor, 2017; Abuelqasim et al., 2017). The geometric corrections with less than half-pixel RMSE (Root Mean Square Error) and atmospheric corrections of images were performed via minimal histogram method.

Using the band combination of Landsat 8 images of the studied area as well as the field observations, the area was divided into nine homogeneous units, in each of which, some points were randomly selected for sampling. Totally, 86 points were selected for the whole region. Subsequently, the coordinates of the points were entered into GPS. The soil samples were taken from a depth of 0-30 in July. Each sample consisted of four sub-samples: one sub-sample in the center and three in three directions, with an angle of 120 degrees (compound sampling) from each other and at a distance of 100 meters from the central sub-sample. This type of sampling is intended

to cover at least nine pixels of the image and minimize the effects of geometric errors. The samples were then transferred to the laboratory (Figure 3).

A B

Figure 2. EM_{38} device

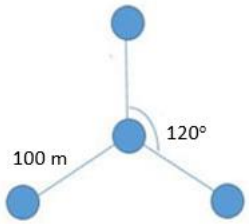

Figure 3. Compound sampling method

In order to determine soil salinity (salinity of saturated paste and apparent electrical conductivity of soil mass) in the study area at the first stage, 86 soil sampling points were taken and at the second stage, using an electromagnetic induction device (EM_{38}), 86 points were read. The number of the readings of each point consisted of two repetitions, in one of which the device had a difference of 90 degrees from the second repetition. Thus, for each point, two readings were made in the horizontal state and two readings were made in the vertical state. By averaging the repetitions of each state, the vertical EM_V, and horizontal EMh readings at each point, the electrical conductivity of soil mass (ECa) was determined. It should be noted that no rainfall was reported from the sampling time until the data recording using EM_{38}. Calibration of EM_{38} is related to the development of appropriate equations for estimating soil salinity by readings of the device. At this stage, several methods have been recommended by various researchers, but the proper method is to calibrate the development of regression equations under local and individual conditions for each unit of work in each region, which was used herein (Rahimian et al., 2010, Huang J. et al., 2014). After being transferred to the laboratory, the soil samples were dried under the laboratory conditions and passed through a 2-mm sieve. Afterwards, some physical and chemical properties were measured using standard methods. The texture was measured via the hydrometric method (Day 1965) and soil acidity was measured in a saturated paste using a fully automatic pH meter (Thomas, 1997). EC was measured in a saturated paste with a conductivity meter in dS / m and apparent electrical conductivity of soil mass (ECa) was measured using EM_{38} (Li et al., 2006). Calcium carbonate was measured by return titration, neutralization of chloride-neutralized

neutralizing matter, and extra titration with soda (Lagacherie et al., 2008). Soluble calcium and magnesium were measured in saturated paste using complex titration (EDTA) method. Soluble sodium and potassium were measured with photometric measurements employing a photometric method (Lagacherie et al., 2008). Carbonate and Bicarbonate were measured via titration of sulfuric acid and equivalent carbonate and bicarbonate were calculated. Bulk density was measured by the clod and paraffin method. Organic carbon was measured through Walky and Black (1934) method. The spectral indices studied herein were calculated utilizing spectral bands of OLI and TIRS (Thermal Infrared Sensor) sensors, as presented in Table 1.

Table 1. Summary of some widely used vegetation and soil salinity indices

Index	Formulation	Reference
NDVI (Normalized Difference Vegetation Index)	$\frac{B5 - B4}{B5 + B4}$	Rouse J. et al. (1974)
VSSI (Vegetation Soil Salinity Index)	2 *B3– 5 * (B4 + B5)	Khan N. M. et al. (2005)
COSRI (Combined Spectral Response Index)	$[\frac{B2+B3}{B4+B5}] * NDVI$	Fernandez-Buces N. et al. (2006)
BI (Brightness Index)	$\sqrt{(B4)^2 + (B5)^2}$	Tripathi N.K. et al. (1997)
SI_1	$\frac{B2}{B4}$	Abbas A. and Khan S. (2007)
SI_2	$\frac{B2 - B4}{B2 + B4}$	Abbas A. and S. (2007)
SI_3	$\frac{B3 * B4}{B2}$	Abbas A. et al. (2007)
SI_4	$\sqrt{B2 * B4}$	Khan S. et al. (2005)
SI_5	$\sqrt{B3 * B4}$	Douaoui A. E. K. et al. (2006)
SI_6	$\sqrt{(B3)^2 + (B4)^2 + (B5)^2}$	Douaoui A. E. K. et al. (2006)
SI_7	$\sqrt{(B3)^2 + (B4)^2}$	Douaoui A. E. K. et al. (2006)
SI_8	$\frac{B2 + B4}{B3}$	Abbas A. and Khan S. (2007)
SI_9	$\frac{B4 + B5}{B3}$	Abbas A. and Khan S. (2007)
SI_{10}	$\sqrt{B4 * B5}$	Abdel Rahman M.A.E (2019)
SI_{11}	$\sqrt{(B4)^2 + (B5)^2}$	Allbed A. et al. (2014)
NDSI (Normalized Differential Salinity Index)	$\frac{(B4 - B5)}{(B4 + B5)}$	Khan S. et al. (2005)
SR (Salinity Ratio)	$\frac{(B4 - B5)}{(B3 + B5)}$	Abdel Rahman M.A.E (2019)

Results and Discussion

Table 2 depicts the summary of statistical data. Table 2 represents the significance level of Kolmogorov-Smirnov and Shapiro-Wilk tests to determine the normality of the data. High standard deviation of salinity values and sodium absorption ratio indicated that the changes in salinity and alkalinity in the region were high. All the data are right-skewed and according to the significance

level (less than 5%) for all the data, the data had no normal distribution. Usually, if the significance level is more than 5%, the data can be assumed to have high normal confidence. As shown in Figures 4 and 6, the variables Vertical EM and salinity have no normal distribution.

Table 2. Statistical summary of the salinity values measured and read via EM_{38}

Significance level								
Shapiro-Wilk	Kolmogorov-Smirnov	Skewness	Standard Deviation	Mean	Max	Min.	n	
0	0	2.05	49.30	56.27	269	6	86	EMV
0	0	2.45	39.57	43.06	235	3.5	86	EMH
0	0	1.89	19.70	11.88	68.10	0.51	86	ECe
0	0	1.76	34.82	24.66	124.50	0.70	86	SAR

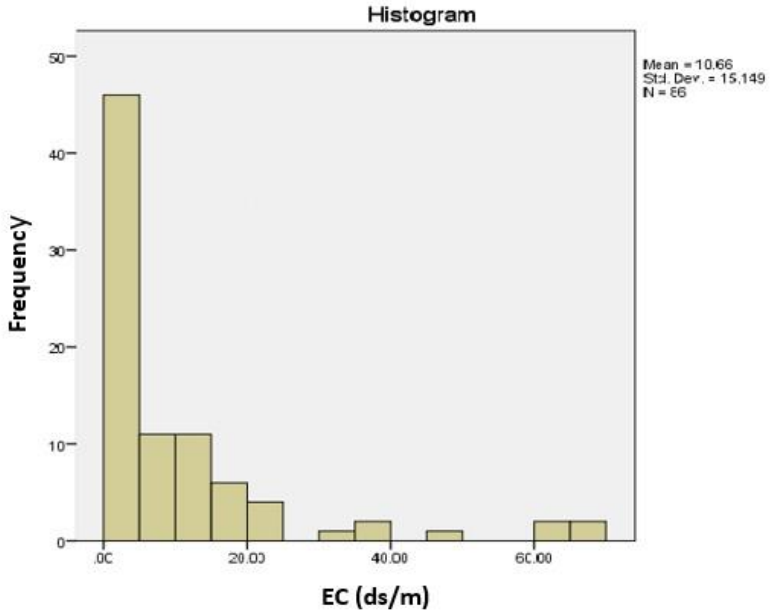

Figure 4. Frequency distribution of EM_v data before normalizing

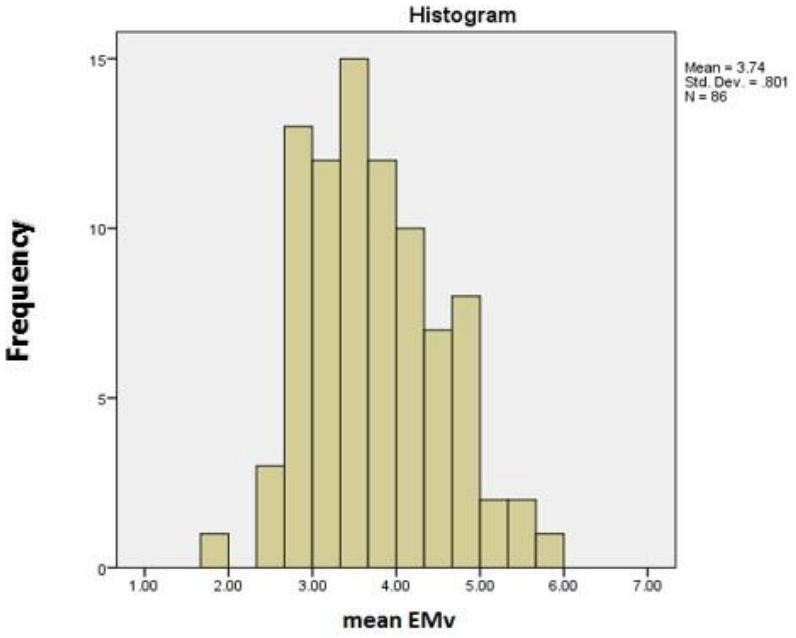

Figure 5. Frequency distribution of EM_v data after normalization

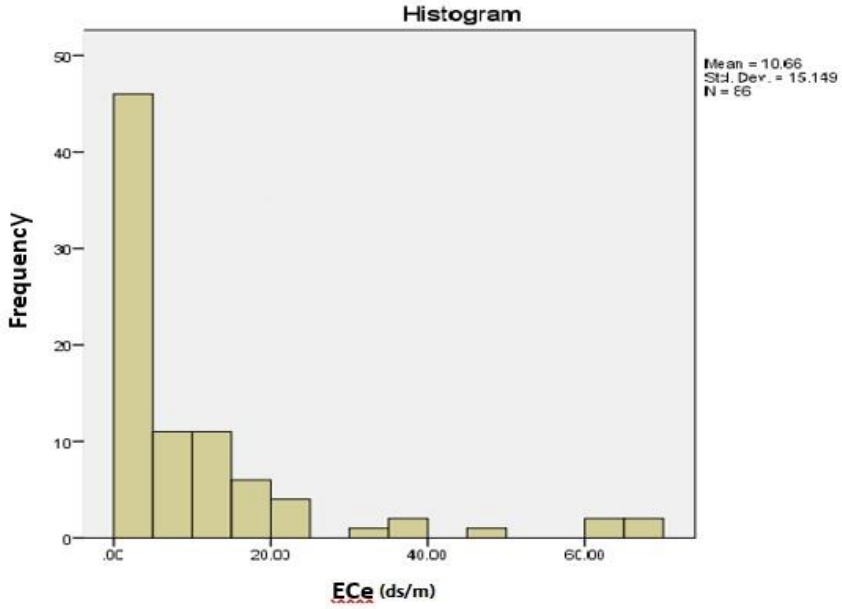

Figure 6. Distribution of ECe data before normalization

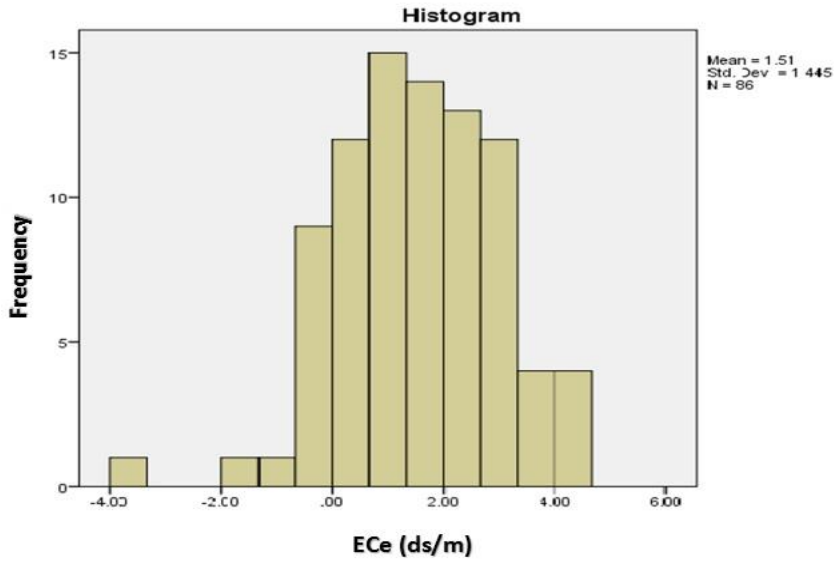

Figure 7. Distribution of ECe data after normalization

Logarithmic transformation was used to normalize the data. Table 3 exhibits the statistical summary of the data after normalization. Accordingly, the data skewness after the normalization reduced and the significance level of both tests of all the data was over 0.05, which indicated the normalization of the data. Figures 5 and 7 illustrate the normal distribution of vertical EM_v and salinity data.

Table 3. Statistical summary of the salinity data and EM_{38} readings after normalization

Significance level			Standard					
Shapiro-Wilk	Kolmogorov-Smirnov	Skewness	Deviation	Mean	Maximum	Minimum	n	
0.36	0.20	0.33	0.80	3.73	5.77	1.79	86	EMv
0.20	0.18	0.23	0.77	3.45	5.46	1.25	86	EMh
0.08	0.08	0.74	1.53	1.25	4.22	-0.67	86	ECe
0.12	0.20	0.22	1.43	2.26	4.82	-0.35	86	SAR

A multivariate linear regression method was used to determine soil salinity via various EM_{38} readings. Table 4 demonstrates regression coefficients between the readings of the electromagnetic conductivity device and soil salinity. The results revealed that the highest coefficient of determination (R^2) belonged to the third equation (0.78). Moreover, the lowest coefficient of determination was observed in the fourth equation (0.68). Table 4 shows that all the equations had high regression coefficients. As could be seen, the coefficient of determination is slightly different with the corrected coefficient of determination R^2_{adj}, indicating the reliability of the equations. Table 4 also represents the best regression equations obtained from the calibration stage of the electromagnetic induction device to estimate soil salinity. Determining the most efficient equations for determination of salinity at the sampling points (37 soil samples) and the accuracy of each of these equations with generalizing to other points without sampling (49 points where only EM_{38} readings were made), it was possible to estimate salinity (ECe) for the 86 points. According to

Table 4,in order to estimate ECe and SAR, Equations (3) and (6) were used, respectively (the highest coefficient of determination).

Table 4. Regression equations between salinity and the horizontal (EM_h) and vertical (EM_v) readings

R^2 Corrected	R^2	R	Equation	No.
0.74	0.75	0.86	ECe = *0.351* EM_h -5.015	1
0.77	0.77	0.88	ECe = *0.284* EM_v - 4.779	2
0.74	0.75	0.87	ECe = (0.617 EM_h) – (0.212 EM_v) – 4.530	3
0.73	0.73	0.85	SAR = 0.616 EM_h - 4.955	4
0.67	0.68	0.82	SAR = 0.490 EM_v - 4.640	5
0.75	0.77	0.87	SAR = (1.560 EM_h) – (0.788 EM_v) – 3.231	6

Determining the significant regression relations between EM_{38} readings and salinity of soil saturation paste, it was also possible to estimation of salinity at unsampled points.Therefore, using these equations, the salinity of soil saturation paste and sodium absorption ratio were predicted for 86 points; the results are summarized in Table 5. The findings revealed that given the significance level of the two relevant tests (less than 0.05) and skewness of above 2 (right- skewness), the data did not have a normal distribution. Figure 7 shows the normalized estimated ECe data. Thus, using logarithmic transformation, the data became close to normal. Normalizing the data, the significance level of the Shapiro-Wilk test for ECe and SAR increased to 0.068 and 0.303, respectively, and the data distribution became close to normal.

Table 5. Statistical summary of ECe and SAR estimated values using horizontal (EM_h) and vertical (EM_v) readings

Significance level		Skewness	Standard Deviation	Mean	Maximum	Minimum	n	Parameter
Shapiro -Wilk	Kolmogorov-Smirnov							
0	0	2.44	15.14	10.65	68.1	0.02	86	ECe
0	0	2.50	26.37	20.11	124.5	0.21	86	SAR

The results obtained herein indicated that ECe had a high correlation (0.928) with SAR and the indices with a high correlation with ECe were SI6, SI11, BI, SI10, and VSSI (Table 6); they are consistent with the results of Khan et al. (2001). They also showed that BI and SI indices are closely correlated with the salinity levels in salt-affected soils. The indices with no significant correlations included COSRI, IR, NDSI, NDVI, SI7, SI8, SI9, SIT, and SR. Furthermore, SI3, SI4, SI5, and SI7 indices had an acceptable correlation. In a study by Ezhirabi et al. (2015) on soil salinity zonation using satellite images in Gorgan, BI and NDSI revealed a high correlation with soil salinity.

After normalizing ECe and the data of all the indices, regression equations were determined using stepwise regression. To this end, ECe was introduced as a dependent variable and indices and measured induced values were introduced as independent variables. Finally, SI6 and SI11 salinity indices and EM_v values were included in the regression model. As shown in Table 7, Equation (1) has a relatively high R^2 and R^2 is slightly different with R^2_{adj}. This indicates that all the independent variables are included in the estimation of dependent variables. Using this model, soil salinity map was calculated and the verification results are exhibited in Table 7.

The classified salinity map, resulted from Equation (1), was assessed with experimental samples (ground truth map). The classification error matrix was calculated and subsequently, the user accuracy, producer accuracy, the total accuracy, and Kappa coefficient were calculated and evaluated with diagonal and non-diagonal pixels of the corresponding Tables (Table 8). Based on

the results, the overall accuracy and kappa coefficient was high, which suggested the high accuracy of the model in estimating salinity and producing a salinity map. Salinity map showed that the central and northern regions had the highest salinity values (S4 ,S3), which corresponded to areas with light crusts, puffy crusts, and sparse vegetation.

Table 6. Correlation of indicators with ECe and SAR after normalization

SAR	ECe	
0.89**	1	ECe
1	0.89**	SAR
0.77**	0.81**	BI
-0.12	-0.14	COSRI
0.77**	0.81**	EMv
0.12	0.18	NDSI
-0.10	-0.13	NDVI
-0.22*	-0.29*	SI1
-0.25*	-0.25*	SI2
0.44**	0.61**	SI3
0.48**	0.54**	SI4
0.48**	0.54**	SI5
0.77**	0.81**	SI6
0.48**	0.54**	SI7
-0.24	-0.18	SI8
0.15	0.14	SI9
0.72**	0.78**	SI10
0.77**	0.81**	SI11
-0.14	0.13	EMh
0.11	0.13	SR
0.67**	0.72**	VSSI

*Significant at a level of 95%

** Significant at a level of 99%

Table 7. Regression relation between the indices and EM_v measurement with ECe

R^2 Corrected	R^2	R	Equation (1)
0.69	0.69	0.75	EC_e = 10.1 EMv – 12.9 SI6 + 3.57 SI11 – 109.27

Table 8. Accuracy classification results

Kappa Index	Overall accuracy	User accuracy	Producer accuracy
83.54	85.75	81.48	83.58

The independent variables of Equation (1) were classified by the maximum likelihood algorithm and the percentage of information classes in the study area was calculated. The results are demonstrated in Figure 9.As could be seen, land use of wheat and alfalfa had the largest area in the region Figure 10 shows the salinity class of all the classified lands. Based on our findings, arable lands could be classified into no salinity to low salinity, which indicated the effect of agricultural operations on leaching of salts and removal of salts from the root environment of plants. The highest level of salinity belonged to the salty lands with white crust classified in the S4 class. This implied the accumulation of salt in the surface soil in the hot season due to the predominance of evapotranspiration over rainfall and the lack of leaching of salts during the year.

As shown in Figure 10, 42.08% of the lands had a salinity problem (Alfalfa land and Wheat grass) and it is expected that the amount increase in the coming years due to the excessive use of

groundwater. Particularly, shallow plowed land seems to be highly prone to becoming an abandoned land.

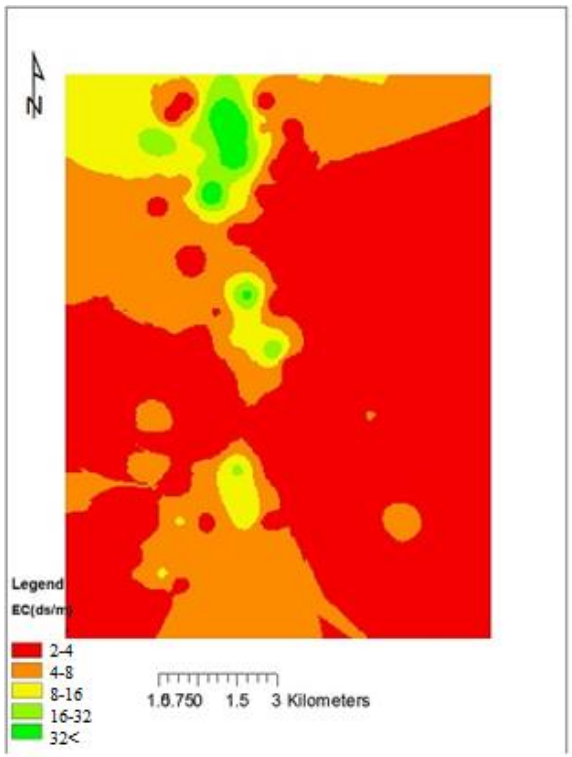

Figure 8. Salinity map calculated based on the model

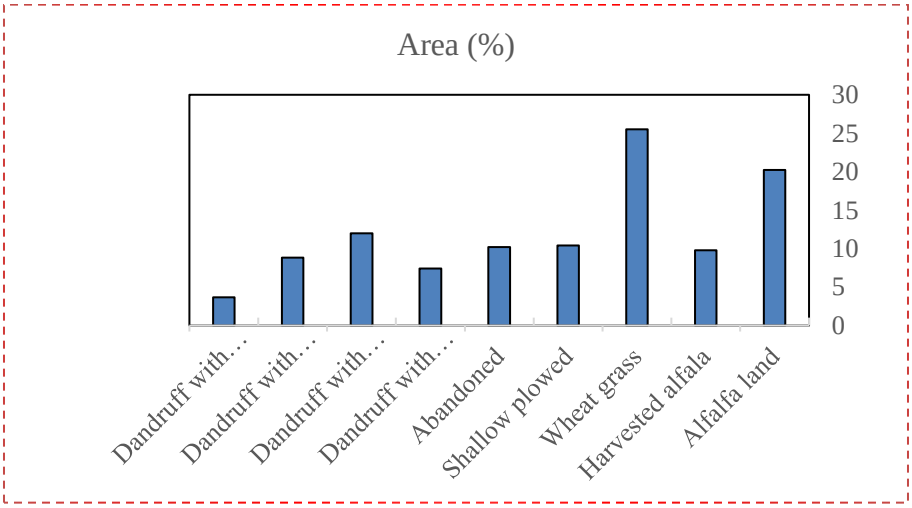

Figure 9. Area percentage of classes

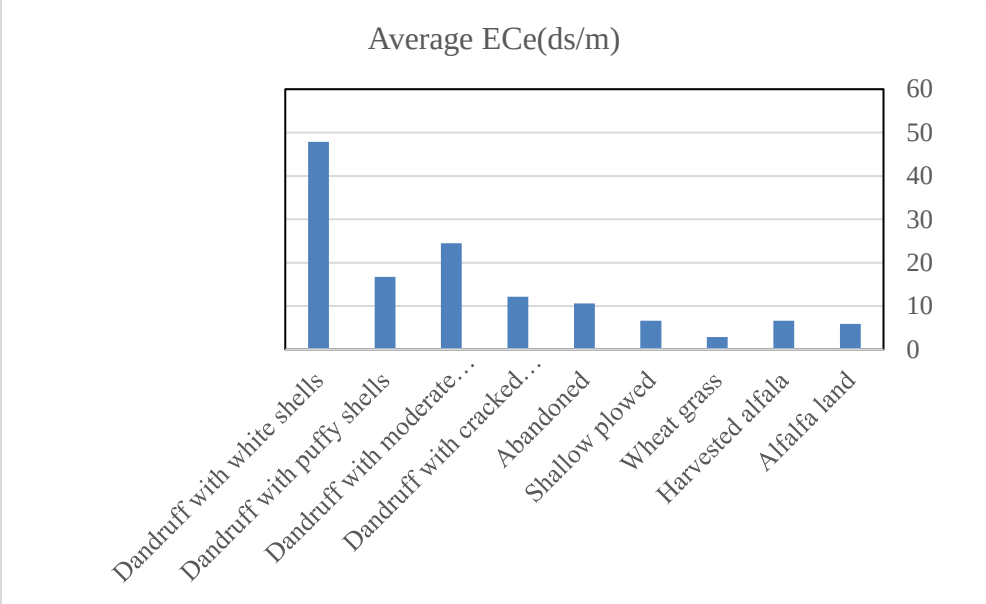

Figure 10. Determination of salinity class for classified land

Table 9. Area of salinity classes

Area (%)	Area (ha)	Explanation	Class
25.52	4392.72	No salinity(EC<4)	S_0
32.38	5573.34	Low salinity(4<EC<8)	S_1
17.61	3031.02	Medium salinity (8<EC<16)	S_2
20.78	3576.87	High salinity(16<EC<32)	S_3
3.68	633.87	Very high salinity (32<EC)	S_4

The results also revealed that about 25% of the land in the region was in the salinity class of very high to high and only 25% was in the no salinity class. Therefore, 50% of the lands are at the risk of salinity intensification (Table 9). In the future, these lands may be classified in the high to very high salinity class.

Conclusions

In the present work, the sampling sites were selected for measurement of salinity using conventional lab techniques and via electromagnetic induction instruments, considering photomorphic approach based upon false color composite and land use patterns. The evaluation capability of Landsat 8 satellite showed that it has the ability to identify saline soils. Analysis of spectral indices implied that soil salinity can be identified in the visible spectrum (blue, green, and red band). Additionally, bands 5, 6, and 7 in the saline soils had spectral interference with moderate vegetation canopy. Of course, these bands could be useful for distinguishing between white and gray crust salty lands. The salt crust lands exhibited the highest reflectance in the reflectance bands of the white and smooth crust. The gray crust had the least spectral reflectance. Distinguishing the abandoned soils from shallow plowed land was also hardly feasible and led to spectral interference and reduced user accuracy for classifying these classes. The obtained results results show that the combination of bands 5 and 6 causes the highest separation of saline crusts and gray crusts. Moreover, SI6 and SI11 salinity indices and EMv values were included in the best regression model and were found to be the most appropriate parameters for calculating the salinity map and spatial

distribution of salinity. Yao Rongjiang and Yang Jingsong (2010) concluded that the estimated salinity of the EM device has a high correlation with the measured salinity and increases the accuracy of salinity measurement in soil layers. The evaluation of the land use classes indicated that wheat and alfalfa crops have the highest area. Furthermore, agricultural lands at low salinity levels (S_0 and S_1) and salty lands with white crust had the highest salinity levels (S_4). In total, 42.8% of the land had salinity problems. In general, this study and other studies on soil salinity monitoring using remote sensing (Fernandez-Buces et al. 2006) shed light on the fact that a combination of remote sensing and EM device measurements contributes to accurately estimating soil chemical properties, including soil salinity. The results also showed salinity indices SI6 and SI11 and vertical measurement of salinity with EM38 device are the most important parameters in modeling soil salinity estimation in arid region and the results of producing soil salinity map with these parameters with an overall accuracy of 85% and kappa coefficient is 0.83, these results demonstrate the success of combining spectral data and salinity measurements with EM38 device.

References

Abbas A, Khan S, Hussain N, Hanjra MA, Akbar S. 2013. "Characterizing soil salinity in irrigated agriculture using a remote sensing approach." Physics and Chemistry of the Earth Parts A/B/C, vol.

Abbas A, Khan S. 2007. Using remote sensing techniques for appraisal irrigated soil salinity. International Congress on Modelling and Simulation (MODSIM), Modelling and Simulation Society of Australia and New Zealand, Brighton.

AbdelRahman M, Metwaly M, Shalaby A. 2019. Quantitative assessment of soil saline degradation using remote sensing indices in Siwa Oasis. Remote Sensing Applications: Society and Environment 13 (2019) 53–60.

Abuelgasim A, Ammad R. 2017. Mapping Sabkha Land surfaces in the United Arab Emirates (UAE) using Landsat 8 data, principal component analysis and soil salinity information. Int. J. Eng. Manuf. 7 (4).

Abuelgasim A, Ammad R. 2019. Mapping soil salinity in arid and semi-arid regions using Landsat 8 OLI satellite data, Remote Sensing Applications: Society and Environment 13 (2019) 415–425.

Alavi Panah S. 2003. Application of remote sensing in Geoscience (Soil Science). University of Tehran, Samt Publications. p. 67-134.

Alavi Panah S. 2006. Remote sensing, principles and application. University of Tehran, Samt Publications.

Allbed A, Kumar L, Aldakheel Y. 2014. "Assessing soil salinity using soil salinity and vegetation indices derived from IKONOS high-spatial resolution imageries: Applications in a date palm dominated region." Geoderma 230: 1-8.

Allbed A, Kumar L. 2013. Soil salinity mapping and monitoring in arid and semi-arid regions using remote sensing technology: a review. Adv Remote Sens 2(December):373–385. https://doi.org/10.4236/ars.2013.24040.

Asfaw E, Suryabhagavan KV, Argaw M. 2016. Soil salinity modeling and mapping using remote sensing and GIS: The case of Wonji sugar cane irrigation farm, Ethiopia." Journal of the Saudi Society of Agricultural Sciences.

Azabdaftari A, Sunarb F. 2016. "Soil salinity mapping using multitemporal Landsat data." in The International Archives of the Photogrammetry, Remote Sensing and Spatial Information Sciences, Volume XLI-B7, 2016 XXIII ISPRS Congress, 12–19 July 2016, Prague, Czech Republic.

Barbiero L, Cunnac S, Mana L, Laperrousaz C, Hammecker C, Maeght JL. 2001. "Salt distribution in the Senegal middle valley: Analysis of a saline structure on planned irrigation schemes from N'Galenka creek." Agricultural Water Management 46(3): 201-213.

Day RP. 1965. Pipette method of particle size analysis. In: Methods of soil analysis. Agronomy 9.ASA USA.p. 553-562.

Douaoui A, Herve N, Walter C. 2006. "Detecting salinity hazards within a semiarid context by means of

combining soil and remote-sensing data." Geoderma 134(1): 217-230.

El Harti A, Lhissou R, Chokmani K, Ouzemou J. 2016. Spatiotemporal monitoring of soil salinization in irrigated Tadla Plain (Morocco) using satellite spectral indices. Int J Appl Earth Obs Geoinf 50:64–73, Elsevier B.V. https://doi.org/10.

Farifteh J, George RJ. 2006. "Assessing salt-affected soils using remote sensing, solute modelling, and geophysics." Geoderma 130(3): 191-206.

Fernandez-Buces N, Palacio JL. 2006. "Mapping soil salinity using a combined spectral response index for bare soil and vegetation: A case study in the former lake Texcoco, Mexico." Journal of Arid Environments 65(4): 644-667.

Forkuor G, Hounkpatin OKL, Welp G, Thiel M. 2017. High Resolution mapping of soil properties using remote sensing variables in South-Western Burkina Faso: a comparison of machine learning and multiple linear regression models. PLoS One 12,e0170478.

Hafyani M, Essahlaoui A, Baghdadi M. Teodoro A, Mohajane M, Hmaidi A, Ouali A. 2019. Modeling and mapping of soil salinity in Tafilalet plain (Morocco). Arabian Journal of Geosciences. 12:35.

Huang J, Wong VNL, Triantafilis J. 2014. Mapping soil salinity and pH across an estuarine and alluvial plain using electromagnetic and digital elevation model data.soil use and management. 30, 394–402

Ibrahim M. 2016. Modeling soil salinity and mapping using spectral remote sensing data in the arid and semi-arid region. Int J Remote Sens Appl 6:76.

Johnston M, Savage MJ, Moolman JH, Plessis HM. 1996. "Calibration models for interpretation of soil salinity measurements using an electromagnetic induction technique." South African Journal of Plant and Soil 13(4): 110-114.

Khan NM, Shiozawa S. 2005. "Assessment of hydrosaline land degradation by using a simple approach of remote sensing indicators." Agricultural Water Management 77(1): 96-109.

Kumar N, Singh SK, Pandey HK. 2018. Appl. Geomath. https://doi.org/10.1007/ s12518-018-0218-2.

Lagacherie P, Baret F, Feret JB, Netto JM, MarcRobbez-Masson J. 2008. Estimation of soil clay and calcium carbonate using laboratory, field and airborne hyperspectral measurements. Remote Sensing of Environment 112 (3: 825-83.

Matinfar HR, Alavi Panah SK, Zand F, Khodaei K. 2011. Detection of soil salinity changes and mapping land cover types based upon remotely sensed data. Arab J Geosci.

Mougenot B. 1993. Effects des sels sur la réflectance et télédétection des sols salés." Cahiers ORSTOM, Serie Pedologie 28: 45-54.

Nawar S, Buddenbaum H, Hill J, Kozak J. 2014. "Modeling and Mapping of Soil Salinity with Reflectance Spectroscopy and Landsat Data Using Two Quantitative Methods (PLSR and MARS)." Remote Sensing, vol. 6, pp. 10813-10834

Rahimian M, Hashminezhad Y. 2010. Calibration of Electromagnetic Inductor (EM_{38}) for evaluation of soil salinity. Journal of Soil Research (Soil and Water Sciences). Volume 24, No. 3. 2010. p. 243-252.

Rahmati M, Hamzepour N. 2017. Quantitative remote sensing of soil electrical conductivity using ETM+ and ground measured data. International Journal of Remote Sensing. 0143-1161 (Print) 1366-5901 (Online) Journal homepage: http://www.tandfonline.com/loi/tres20.

Rao B, Sankar T, Dwivedi R, Thammappa S, Venkataratnam L, Sharma R, Das S. 1995. Spectral behaviour of salt-affected soils. Inter. J. Rem. Sens. 16: 2125-2136.

Rongjiang R, Jingsong Y. 2010. Quantitative evaluation of soil salinity and its spatial distribution using electromagnetic induction method. AgriculturalWater Management.97:1961-1970

Rouse Jr, John W. 1974. "Monitoring the vernal advancement of retrogradation of natural vegetation, Final report, Greenbelt, MD." National Aeronautics and Space Administration (NASA), Goddard Space Flight Center (GSFC).

Sharma D, Gupta S. 2000. Application of EM38 for soil salinity appraisal: an Indian experience. EM38 Workshop, New Delhi, India.

Song CC, Yan BX, Song XS. 2002. The electromagnetism technology application in the sodium-saline soil. Scientia Geographica Sinica, 22(1), 91-95, (in Chinese).

Thomas DSG. 1997. Arid zone Geomorphology: Process, Form and Change in Drylands (Second edition). John Willey & Sons Inc. 713 pp.

Tripathi NK, Rai BK, Dwivedi P. 1997. Spatial modeling of soil alkalinity in GIS environment using IRS data. Proceedings of the 18th Asian conference on remote sensing, Kualalampur, pp. 1–6.

Walky A, Black I. 1934. An examination of the Degtiareff method for determining soil organic matter and proposed modification of the chromic acid titration method. Soil Science, 63, 29-38.

Williams BG, Baker GC. 1982. An electromagnetic induction technique for reconnaissance surveys of soil salinity hazards. Australian Journal of Soil Research, 20, 107–118.

Yu R, Liu T, Xu Y, Li C. 2010. "Analysis of salinization dynamics by remote sensing in Hetao IrrigationDistrict of North China." Agricultural Water Management 97(12): 1952-1960